A TEST STAND FOR QUANTIFYING THE CORE GAS RELEASE AND THE GAS PERMEABILITY OF INORGANICALLY-BOUND FOUNDRY CORES

Benedikt Kirchebner , **Simon Kammerloher** , **Georg Fuchs** , **Erwin Reberger** , **Wolfram Volk** and **Philipp Lechner**
Chair of Metal Forming and Casting, Department of Mechanical Engineering, TUM School of Engineering and Design, Technical University of Munich, Garching, Germany

Abstract

Environmental and work safety aspects necessitate a radical change in the foundry industry. Organic binder systems for foundry sand cores create toxic combustion products and are, therefore, more and more often substituted by inorganic binder systems. While providing an environmental advantage by mainly releasing water vapor, inorganic binder systems impose new challenges for the casting process. The gas release of inorganically-bound foundry cores can lead to increased gas porosity in the cast parts and thus to high scrap rates. The present work aims to gain more understanding of the gas generation and transport in inorganic sand binder systems. We developed a test stand to measure the temperature-dependent core gas release in inorganically-bound foundry cores and their gas permeability. Samples were prepared in a core blowing process and analyzed using the test stand. The measurement results are in good agreement with validation experiments and existing literature.

Keywords: foundry core, inorganic binder, organic binder, core gas, permeability, core blowing

Introduction

In metal casting, expendable molds and foundry cores are typically made from bonded sand. In the past decades[1] and to this day,[2] organic substances are often used as a bonding agent. Commonly used organic binders are furans, alkaline phenolics, and phenol-urethanes.[3] The main problem with these binders is the release of toxic waste gases when they come into contact with melt.[4] The pyrolysis products of furans,[5] alkaline phenolics,[6] and phenol-urethanes[7] contain many problematic substances that are heavily air polluting, toxic, carcinogenic, and mutagenic. Further details on the decomposition substances of organic binders are described in the literature.[8]

In contrast with these organic binders, inorganic water glass binders mainly release water vapor.[9] For some inorganic binders, due to additives, harmful decomposition products still occur, but their content is reduced drastically.[10]

Thus, inorganic binding agents are increasingly being used.[11] Unfortunately, inorganically-bound cores and molds pose a variety of challenges. For example, mechanical stability,[12] especially with regard to humidity,[13] and the decoring behavior[14] have to be considered. Further, the susceptibility to pores in the casting is higher due to the different physical principles of gas generation. If the gas pressure in the core exceeds the counterpressure of the melt during casting and gas permeability of the core is limited, the gas escapes not only via the core bearings or via any vents provided. If the melt has not yet solidified, the gas can also escape through the melt, thus leading to porosities.[15]

Since the foundry industry depends on stable casting processes, extensive knowledge of the behavior of inorganically-bound foundry cores is crucial. Casting processes are influenced by many factors, e.g., casting temperature, filling speed, mold orientation, and core geometry. For blowhole-free casts, the gas transport shall occur through the core bearings with no gas escape into the melt. A material model for the gas release of inorganically-bound foundry cores shall assist in optimizing the processing conditions to eventually avoid blowholes.

Our goal was to develop a test stand for quantifying the core gas release and gas permeability without having to perform costly and elaborate test casts with melt. The measurements performed with this test stand shall build the foundation for the material model. The test stand's analyses were validated by comparing the obtained results with an existing measurement device and literature.

Theoretical Background

Gas Generation in Organic and Inorganic Binders

In the casting process, foundry cores and consequently the binder come into contact with molten metal. The binders decompose and release various substances. Furans, alkaline phenolics, and phenol-urethanes release many substances, which remain gaseous even at lower temperatures.[16] In contrast, inorganic binders mainly release water vapor, which condensates at temperatures below 100 °C. Consequently, if some of the water vapor formed reaches inner areas of the core with temperatures below 100 °C, it turns liquid, thus reducing the amount of gas present in the core, i.e., the gas pressure. Accordingly, in inorganic cores, gas transport must be considered in addition to gas generation in order to study porosity caused by gas escape.[17]

It shall be noted that the use of a constant condensation temperature (100 °C) is a simplification since the condensation temperature always depends on the prevailing pressure. We assume that the gas pressure in the core does not increase to a degree where we have to consider this effect. Firstly, because of the gas flow through the core bearings and, secondly, because of a possible gas flow through the melt, which is at a comparatively low pressure in casting processes with sand cores.

Moisture Transport in Porous Materials

To explain moisture transport in the context of metal casting, we will first consider a foundry core that is completely surrounded by melt. In the peripheral area of the foundry core at a short distance from the melt, the temperature rises above 100 °C, causing the water present there to evaporate and locally increase the pressure in the molding material. Due to the counterpressure of the melt and the lower pressure in the colder areas of the molding material, the water vapor flows in accordance with the pressure and temperature gradient into areas of the core further away from its surface. If the ambient temperature of the steam falls below 100 °C, the moisture begins to condense, releasing heat to the surrounding molding material. Thus, in addition to heat conduction, convection also plays an important role in the temperature distribution in the molding material.[17]

As already described, the moisture transport is characterized by a cascade of evaporation and condensation. Related to Campbell,[17] the area of interest can be divided into five zones:

- *Dry sand zone*. Here, the temperatures are above 100 °C, and all moisture is evaporated.
- *Evaporation zone*. Moisture is evaporating. The temperature is at 100 °C.
- *Vapor transport zone*. At essentially uniform temperatures of 100 °C, steam is migrating toward the condensation zone.
- *Condensation zone*. Here, the steam condenses and adds moisture.
- *Moist sand zone*. Areas with sand at temperatures below 100 °C, unaffected by steam, yet.

In Figure 1, the five zones are visualized with a plot of the qualitative moisture content in the respective zone.

Gas Shock

Initially, only a low gas pressure builds up in the foundry core due to the continuous condensation of moisture. Consequently, the moisture inside the foundry core does not escape through the melt, but accumulates in cold areas.[17] When the temperature in the coldest region rises to over 100 °C, the moisture will vaporize, thus increasing the gas pressure drastically, until the counterpressure of the melt is eventually reached. From this point on, the core gas escapes through the melt, causing porosities in the cast part, so called blowholes.[15] The effect of a time-delayed, abrupt rise of the pressure inside the core is referred to as *gas shock*.

The goal in optimizing the casting conditions is to prevent gas shock-induced blowholes, e.g., by ensuring the melt has already solidified in regions where a gas shock occurs.

Gas Permeability

There are multiple theories and mathematical descriptions for the flow of a fluid through porous materials.[18] For incompressible fluids and laminar flow, Darcy's law is commonly used.[19] This empirical law can be stated as

$$K = \frac{Q \cdot \eta \cdot l}{\Delta p \cdot A} \qquad \text{Eqn. 1}$$

where K is the permeability, Q is the volumetric flow rate, η is the dynamic viscosity of the fluid, l and A are the length and cross-sectional area of the flowed through body, respectively, and Δp is the pressure drop due to the flow through the porous body.[20] For general cases, e.g., faster flow speeds, more advanced mathematical formulations are available.[21] The Reynolds number
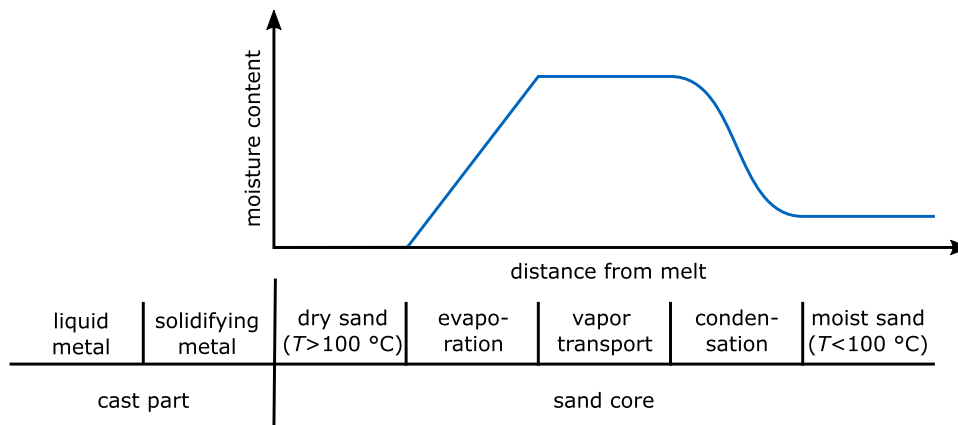
Figure 1. Schematic of the water transport in inorganic foundry cores. The metal conducts heat to the core material and heats up the binder material. At 100 °C, the bound water evaporates and condensates in cooler areas. The water is transported into a cold spot and evaporates abruptly when the temperature exceeds 100 °C (gas shock).[17]

$$Re = \frac{\rho \cdot d \cdot v}{\eta} \qquad \text{Eqn. 2}$$

where ρ is the density of the fluid, d is the mean grain diameter, v is the average flow velocity, and η is the kinematic viscosity of the fluid used to determine if Darcy's law can be used to describe the fluid flow.[22] Darcy's law is typically applied if $Re < 1$[23], while some authors state a Darcy regime of $0 \leqslant Re \leqslant 4$.[24] In the case of argon at room temperature as a fluid, a sample diameter of 25 mm, and a mean grain diameter of 0.3 mm, the Reynolds number is less than one for flow speeds $Q/A \lesssim 0.04$ m/s and less than four for flow speeds $Q/A \lesssim 0.17$ m/s. In the case of water vapor at 100 °C as a fluid and the same sample diameter and mean grain diameter, the Reynolds number is less than one for flow speeds $Q/A \lesssim 0.07$ m/s and less than four for flow speeds $Q/A \lesssim 0.27$ m/s.[25]

It shall be noted that fluid flow is a complex matter, and for more precise considerations, the Knudsen number[26], for example, would also have to be taken into account[27], which is neglected in this work.

Materials and Methods

Experimental Setup

Core Gas and Permeability Test Stand

For the measurement of the core gas release and gas permeability, a test stand was developed. Since the samples are heated by an induction heating system, the test stand is also referred to as Induction Analysis Furnace (IAF). An

Figure 2. Induction Analysis Furnace (IAF) that is used to perform the core gas release and gas permeability measurements.

overview and inside view of the IAF is shown in Figures 2 and 3.

The system mainly consists of an argon-purged, water-cooled high-temperature oven and a personal computer (PC) with isolated cores for running the real-time capable control software with a graphical user interface (TwinCAT 3, Beckhoff Automation GmbH & Co. KG, Verl, Germany). The oven is equipped with a 6 kW induction heating system (COBES GmbH, Ettenheim, Germany) and two pyrometers (Optris CTlaser LT CF4 and CTlaser 2MH1 CF4, Optris GmbH, Berlin, Germany) that, in combination, cover the temperature range of -50 °C to 2000 °C. The induction heating and the pyrometer system are controlled in closed-loop, thus enabling a precise and contact free heating of the crucible. A regulating system for both gas flow and pressure enables the purging of the oven
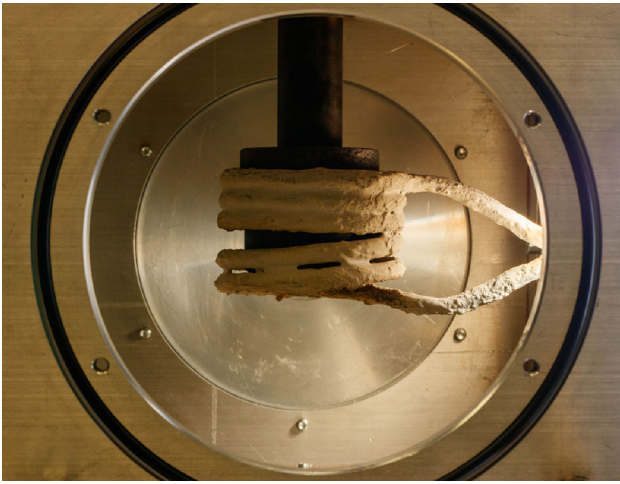
Figure 3. Inside view of the Induction Analysis Furnace (IAF). The induction coil is covered by a ceramic layer to protect it from heat radiation.

with argon at a user-defined flow rate while keeping a user-defined pressure inside the chamber. The regulating system consists of a flow meter (SFAH-100U-Q8S-PNL, Festo Vertrieb GmbH & Co. KG, Esslingen, Germany), a proportional flow valve (ASCO Preciflow IPC, Emerson Electric Co., Ferguson, USA), and a proportional pressure control valve (AirTronic$^®$ D, PPA10-A500, AirCom Pneumatic GmbH, Ratingen, Germany). The oven is further equipped with an oxygen sensor (FCX-TR0025-7-5-Q08-113-000, Angst+Pfister Sensors and Power AG, Zurich, Switzerland) with a measurement range of $0\% - -25\%$ and an accuracy of $\pm 0.5\%$ (full scale) to determine the oxygen concentration inside the chamber. In combination with the proportional flow valve, the oxygen sensor is used in closed-loop control. Further, a temperature sensor and an overpressure valve are attached to the oven. The power for the test stand is distributed and fused via two separate electric cabinets, thus minimizing electromagnetic interference. One cabinet is used for high-voltage applications, i.e., powering the induction heating system, the water cooling aggregate, the vacuum pump, and the PC with its display. The second cabinet is used for powering the sensors and valves. A schematic of the test stand is depicted in Figure 4.

The test stand can be operated in two different modes: one for measuring the core gas release and another for measuring the gas permeability. For the two modes, the same sample type can be used but the setup has to be changed as described in the following.

The core gas release measurement system consists of a heated pipe that is attached to the crucible and submerges into a water reservoir. The pipe is equipped with a thermocouple and heating wire to closed-loop control the temperature of the pipe in order to keep water vapor inside the pipe from condensing. The vapor travels through the

pipe and eventually condenses in the water reservoir, thus increasing the mass of the reservoir. With a XSR304 laboratory balance (Mettler-Toledo GmbH, Giessen, Germany) with a reading accuracy of 0.1 mg, the change in mass is detected and continuously tracked. The sample is located in a graphite crucible and heated via induction (see Figure 5). On the bottom part of the crucible, an end piece is screwed on to prevent the escape of core gas. On the top part, the crucible is connected to the heated pipe. The chamber is purged with argon, controlled by the flow meter and a proportional pressure regulator.

For measuring the gas permeability, the end piece is not screwed onto the sample, and the relative pressure inside the chamber is varied between 0 bar and 0.44 bar. The setup is changed so that the resulting gas flow through the sample does not enter the heated pipe but instead a flow meter (SFAH-100U-Q8S-PNL, Festo Vertrieb GmbH & Co. KG, Esslingen, Germany). Thus, the pressure-dependent gas flow can be measured.

The essential advantage of our test stand is that the experiments can be run under controlled conditions (atmosphere, temperature, and pressure) and that it replaces costly and elaborate test casts with melt.

Moisture Balance

For validating the experimental results of the core gas generation measurements, a KERN DBS 60-3 moisture balance (KERN & SOHN GmbH, Balingen-Frommern, Germany) is used. The balance has a maximum total sample mass of 60 g and a repeatability of 1 mg. The maximum operating temperature of the balance is 200 °C. The moisture content is evaluated in mass-% at a readability of 0.01 %. The signal is continuously logged via the RS232 interface.

Sample Description and Preparation

Three different sample types, denoted with ST1, ST2, and ST3, are analyzed. ST1 is a cylinder with a nominal dimension of 50.5 mm in diameter and 50 mm in length. ST2 is a sand sample inside a graphite crucible with 50 mm in outer diameter, 40 mm in inner diameter, and a length of 50 mm. Similarly, ST3 is a sand sample inside a graphite crucible with 50 mm in outer diameter, 25 mm in inner diameter, and a length of 50 mm. The three samples are depicted in Figure 6.

The samples for all measurements are prepared in a core blowing process using a Loramendi SLC2-25L (Loramendi S.Coop., Vitoria, Spain). The graphite crucibles of ST2 and ST3 are directly used as tool inserts. Silica sand (H32, Quarzwerke GmbH, Frechen, Germany) with a mean grain
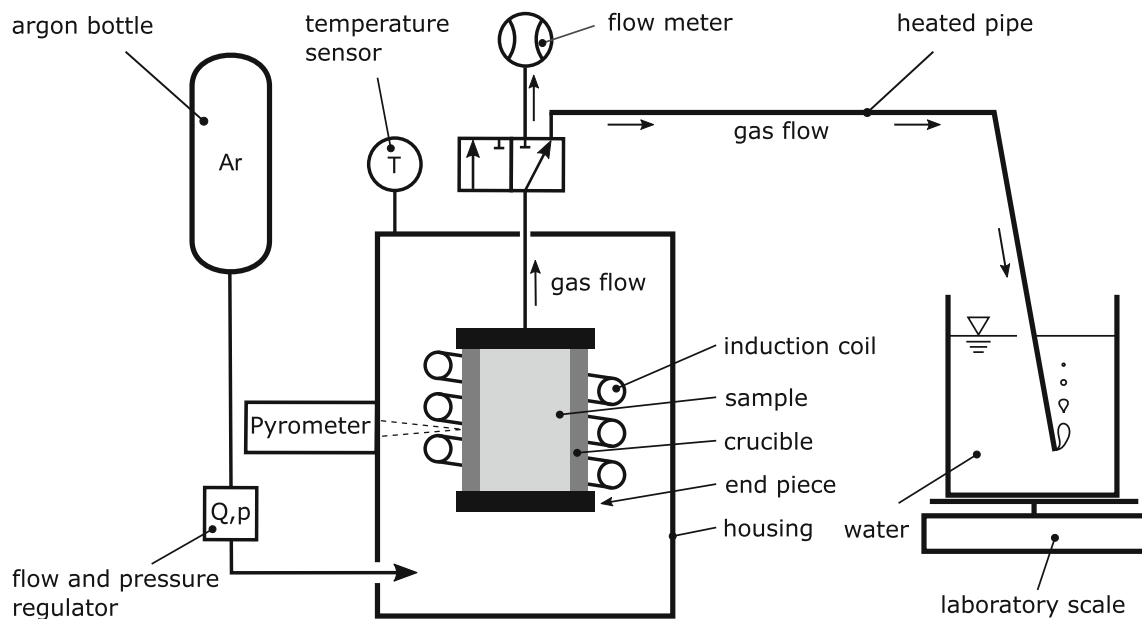
Figure 4. *Schematic of the Induction Analysis Furnace (IAF). The sample is located in a graphite crucible and heated via induction. The bottom part of the crucible is terminated with an end piece to prevent the escape of core gas. On the top part, the crucible is connected to the heated pipe. The chamber is purged with argon, controlled by the flow meter and a proportional pressure regulator. The core gas is transported in a heated pipe ($T > 100°C$) to prevent condensation. The pipe immerses into a water-filled glass container that is placed onto laboratory scales.*

Figure 5. *Inductively heated graphite crucible. View through the sight glass of the Induction Analysis Furnace (IAF).*

Figure 6. *The three different sample types that are analyzed in this work. From left to right: ST1, ST2, and ST3.*

Table 1. *Core Blowing Process Settings*

Parameter	Value
Tool temperature	150 °C
Gassing temperature	220 °C
Blowing pressure	5 bar
Blowing time	1 s
Pre-gassing time	10 s
Gassing time	5 s

diameter of $320\,\mu$ m and a two component inorganic binder (INOTEC EP 4158 and INOTEC PROMOTOR TC 4500, ASK Chemicals, Hilden, Germany) are used. For the preparation of the samples of this work, 2.5wt% binder and 2wt% promotor are added to the sand. The processing parameters for the core blowing process are listed in Table 1. All values are set values.

The density of the blown samples was evaluated by blowing three cylinder samples and measuring their respective weight. The end pieces of the samples were filed off to obtain flush cylinder faces. The diameter and length were measured using calipers with a reading accuracy of

0.05 mm. The weight was measured using the XSR304 laboratory balance. All samples showed a diameter of 50.5 mm and a height of 50.0 mm. The samples weight was determined as 159.6 g, 158.6 g, and 158.7 g (rounded to one decimal place, respectively). Assuming a homogeneous density, this leads to an average density of 1.59 g/cm^3. Consequently, the net foundry core mass of ST2 and ST3 is 99.9 g and 39.0 g, respectively.

Experimental Procedure

Measurement of Gas Release

For gas generation measurements with the IAF, an ST2 sample is mounted in the test stand, and the bottom cap is screwed on. The induction heating is activated, and temperature of the graphite crucible is measured via the pyrometers. The heating rate is 50°C/min, related to the surface of the graphite crucible. The core heats up and releases the core gas, which travels through the heated pipe and condenses in the water reservoir. The water reservoir mass is recorded over time, synchronous with the sample's temperature.

For the validation experiments, an ST1 sample is taken, and approximately 10 g are filed off the sample. These 10 g of loose sand with binder are placed in the moisture balance. The moisture balance heats up to a temperature of 200 °C and records the weight loss in mass-%. The weight loss value after a time of 5 min is used for the validation. In total, four ST1 samples are measured for the validation.

Measurement of Gas Permeability

For gas permeability measurements with the IAF, an ST3 sample is mounted in the test stand without the bottom cap. The flow path of the core gas is changed to flow through the flow meter, rather than the heated pipe. Via the flow and pressure regulator, an increasing pressure is applied, and the argon flow after the sample is recorded over time, synchronous with the pressure inside the chamber. The gas permeability measurements on the IAF can be performed with both ST2 and ST3 samples. However, all measurements were performed with ST3 samples for reasons of availability. In total, three ST3 samples are measured.

Results and Discussion

Results of the Gas Release Measurements

One representative curve for the released gas mass m is depicted in Figure 7. Due to a transient heating, the sample's temperature is expected to be, inhomogeneous during heating. To avoid confusion, the values in Figure 7 are
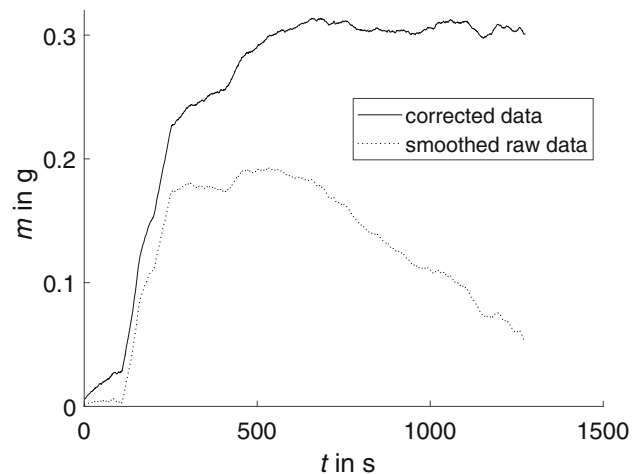
Figure 7. Plot of the released gas mass m with respect to the measurement time t. The smoothed raw signal is displayed as a dotted line; the corrected signal is displayed as a solid line.

plotted with respect to the measurement time t rather than the temperature, since the applied heating rate of 50°C/min refers to the crucible's surface rather than a homogeneous sample temperature.

The smoothed raw data are shown as a dotted line. The constant rate weight loss is due to evaporation of water in the reservoir that is exposed to air at room temperature. This constant drift is determined by fitting the quasi-linear part from $t = 900s$ until the end of the measurement. The linear fit is used to correct the smoothed raw data. The result of this correction is shown in the solid line. For comparison with the validation experiments, the maximum value of the corrected curve is taken into account.

The three gas release measurements lead to maximum released gas masses of 0.314 g, 0.428 g and 0.305 g, resulting in a mean value of 0.349 g and a standard deviation (SD) of 0.056 g. With respect to the calculated average mass of an ST2 sample, the mass percentage of the gas release quantity is 0.31 %, 0.42 % and 0.31 %, respectively. The measurement results are listed in Table 2.
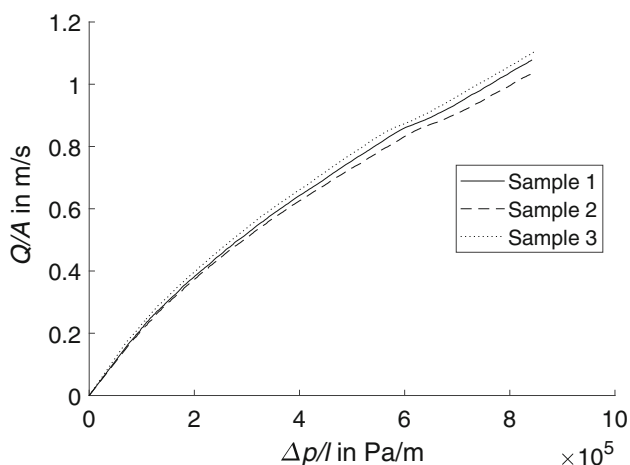
Results of the Gas Permeability Measurements

The results of the measurements of the gas permeability with the IAF are shown in Figure 8 where the flow speed Q/A is shown with respect to the sample length-specific pressure difference p/l. The solid, dashed, and dotted lines represent the three different measurements. Because of the operating range of the pressure regulating system, the values for fluid flow rate between 0 l/min and 5 l/min are extrapolated linearly toward a flow rate of 0 l/min at a pressure difference of 0 bar. It is assumed that we fall into the linear Darcy regime.

Table 2. Results of the Gas Release Measurements With the Induction Analysis Furnace (IAF) and the Moisture Balance

	Gas quantity (IAF)	Gas quantity (IAF)[1]	Gas quantity (moisture balance)
Measurement 1	0.314 g	0.31%	0.38%
Measurement 2	0.428 g	0.42%	0.39%
Measurement 3	0.305 g	0.31%	0.43%
Mean	0.349 g	0.35%	0.40%
SD	0.056 g	0.06%	0.02%

[1]With respect to the calculated average mass of an ST2 sample

Figure 8. Result of three gas permeability measurements. The flow speed Q/A is shown with respect to the sample length-specific pressure difference p/l. The solid, dashed, and dotted lines represent the three different measurements.

The results are validated by comparing with existing literature. Ettemeyer et al.[28] performed permeability measurements of samples with the same geometry, sand and binder system but with less total binder content (3.9 % vs 4.5 %). For a specific pressure difference $\Delta p/l$ of 10^5 Pa/m, an average flow speed of $Q/A = 0.22$ m/s (SD < 0.01 m/s) was obtained with our test stand, in comparison with a measured range $Q/A \approx 0.15$ m/s to $Q/A \approx 0.7$ m/s obtained by Ettemeyer et al. At a specific pressure difference $\Delta p/l$ of 5×10^5 Pa/m, we obtained an average flow speed of $Q/A = 0.75$ m/s (SD < 0.02 m/s) in comparison with a measured range $Q/A \approx 0.5$ m/s to $Q/A \approx 1.1$ m/s obtained by Ettemeyer et al.

Taking the different binder contents into account, the results of our test stand seem plausible. Furthermore, the results of our test stand show far less scatter.

Summary and Conclusions

Because of environmental and work safety aspects, the foundry industry is more and more often substituting organic binder systems for inorganic binder systems. While eliminating the harmful emissions of the organic binder systems, the inorganic binder systems introduce new challenges to the production processes. One of them is gas porosities that stem from the abrupt release of core gas (gas shock).

We suggest using a simulation approach to optimize the processing conditions for casting with inorganically-bound foundry cores, eventually reducing gas shock-induced blowholes in cast parts. For creating a material model, extensive knowledge of the behavior of foundry core materials is necessary. Since test casts are costly and elaborate, we developed a test stand for quantifying the core gas release and the gas permeability of inorganically-bound foundry cores. First measurement results are in good agreement with validation experiments and existing literature. This provides the basis for a comprehensive quantification of commonly used inorganic binder systems.

The next steps are running large-scale analyses of industrially used sand and binder materials. The measured data will be used to build the material model, which eventually shall enable the optimization of the casting process.

Open Access

REFERENCES

1. S. Saetta, V. Caldarelli, Lean production as a tool for green production: the green foundry case study. Procedia Manuf. **42**, 498–502 (2020). https://doi.org/10.1016/j.promfg.2020.02.042

2. S.G. Acharya, J.A. Vadher, M. Sheladiya, A furan no-bake binder system analysis for improved casting quality. Int. J. Metalcast. **10**(4), 491–499 (2016). https://doi.org/10.1007/s40962-016-0059-x

3. P. Wan, J. Zhou, Y. Li, Y. Yin, X. Peng, X. Ji, X. Shen, Kinetic analysis of resin binder for casting in combustion decomposition process. J. Therm. Anal. Calorim. **147**(11), 6323–6336 (2022). https://doi.org/10.1007/s10973-021-10902-3

4. Polzin, H.: Inorganic Binders: For Mould and Core Production in the Foundry, 1. ed. edn. Schiele & Schön, Berlin (2014). https://permalink.obvsg.at/AC16559702

5. M. Holtzer, A. Kmita, S. Żymankowska-Kumon, A. Bobrowski, R. Dańko, Influence of the hardener on the emission of harmful substances from moulding sands with furan resin in the pyrolysis process. Arch. Foundry Eng. **16**(1), 107–111 (2016). https://doi.org/10.1515/afe-2016-0012

6. A. Kmita, C. Fischer, K. Hodor, M. Holtzer, A. Roczniak, Thermal decomposition of foundry resins: A determination of organic products by thermogravimetry-gas chromatography-mass spectrometry (tg-gc-ms). Arab. J. Chem. **11**(3), 380–387 (2018). https://doi.org/10.1016/j.arabjc.2016.11.003

7. R.S. Dungan, J.B. Reeves III., Pyrolysis of foundry sand resins: a determination of organic products by mass spectrometry. J. Environ. Sci. Health, Part A **40**(8), 1557–1567 (2005). https://doi.org/10.1081/ESE-200060630

8. M. Kubecki, M. Holtzer, A. Bobrowski, R. Dańko, B. Grabowska, S. Żymankowska-Kumon, Analysis of the compounds from the btex group, emitted during thermal decomposition of alkyd resin. Arch. Foundry Eng. **12**(3), 69–74 (2012). https://doi.org/10.2478/v10266-012-0084-z

9. A. Siewiorek, R. Nowaka, A. Chojeckib, J. Mocek, Gas evolution rate from heated moulding sands bonded with organic binders. Arch. Foundry Eng. **11**(1), 87–92 (2011)

10. A. Bobrowski, M. Holtzer, S. Żymankowska-Kumon, R. Dańko, Harmfulness assessment of moulding sands with a geopolymer binder and a new hardener, in an aspect of the emission of substances from the btex group. Arch. Metall. Mater. **60**(1), 341–344 (2015). https://doi.org/10.1515/amm-2015-0056

11. E. Weissenbek, J. Willimayer, J. Wolf, Bmw-leicht-metallgießerei setzt auf anorganisch gebundene kerne. Gießerei **95**(6), 30–33 (2008)

12. P. Lechner, C. Hartmann, F. Ettemeyer, W. Volk, A plane stress failure criterion for inorganically-bound core materials. Materials **14**(2), 247 (2021). https://doi.org/10.3390/ma14020247

13. A. Fortini, M. Merlin, G. Raminella, A comparative analysis on organic and inorganic core binders for a gravity diecasting al alloy component. Int. J. Metalcast. **16**(2), 674–688 (2022). https://doi.org/10.1007/s40962-021-00628-1

14. F. Ettemeyer, M. Schweinefuß, P. Lechner, J. Stahl, T. Greß, J. Kaindl, L. Durach, W. Volk, D. Günther, Characterisation of the decoring behaviour of inorganically bound cast-in sand cores for light metal casting. J. Mater. Process. Technol. **296**, 117201 (2021). https://doi.org/10.1016/j.jmatprotec.2021.117201

15. Monroe, R.: Porosity in castings. ChemInform **37**(42) (2006). https://doi.org/10.1002/CHIN.200642218

16. P. Wan, J. Zhou, Y. Li, Y. Yin, D. Huang, X. Ji, X. Shen, Experimental study on gas evolution process of binders in foundry industry based on tg-ms. Procedia Manuf. **37**, 311–318 (2019). https://doi.org/10.1016/j.promfg.2019.12.053

17. Campbell, J.: Complete Casting Handbook: Metal Casting Processes, Techniques and Design, Butterworth-Heinemann, Oxford (2011)

18. Lage, J.L.: The fundamental theory of flow through permeable media from darcy to turbulence. In: Transport Phenomena in Porous Media, pp. 1–30. Pergamon, Oxford (1998). https://doi.org/10.1016/B978-008042843-7/50001-5

19. M. Honarpour, S.M. Mahmood, Relative-permeability measurements: an overview. J. Petrol. Technol. **40**(08), 963–966 (1988). https://doi.org/10.2118/18565-PA

20. D. Sundaram, J.T. Svidró, A. Diószegi, J. Svidró, Measurement of darcian permeability of foundry sand mixtures. Int. J. Cast Met. Res. **34**(2), 97–103 (2021). https://doi.org/10.1080/13640461.2021.1917890

21. K. Boomsma, D. Poulikakos, The effects of compression and pore size variations on the liquid flow characteristics in metal foams. J. Fluids Eng. **124**(1), 263–272 (2002). https://doi.org/10.1115/1.1429637

22. L. Wang, Y. Li, G. Zhao, N. Chen, Y. Xu, Experimental investigation of flow characteristics in porous media at low reynolds numbers (re→0) under different constant hydraulic heads. Water **11**(11), 2317 (2019). https://doi.org/10.3390/w11112317

23. M.R. Tek, Development of a generalized darcy equation. J. Petrol. Technol. **9**(6), 45–47 (1957)

24. M. Firdaouss, J.L. Guermond, P. Le Quéré, Nonlinear corrections to darcy's law at low reynolds numbers. J. Fluid Mech. **343**, 331–350 (1997)

25. VDI-Gesellschaft Verfahrenstechnik und Chemiein- genieurwesen: VDI-Wärmeatlas. Springer Berlin Heidelberg, Berlin, Heidelberg (2013). https://doi.org/ 10.1007/978-3-642-19981-3

26. M. Knudsen, Die gesetze der molekularströmung und der inneren reibungsströmung der gase durch röhren. Ann. Phys. **333**(1), 75–130 (1909). https://doi.org/10. 1002/andp.19093330106

27. L.M. De Socio, L. Marino, Gas flow in a permeable medium. J. Fluid Mech. **557**, 119–133 (2006). https:// doi.org/10.1017/S0022112006009621

28. F. Ettemeyer, P. Lechner, T. Hofmann, H. Andrä, M. Schneider, D. Grund, W. Volk, D. Günther, Digital sand core physics: predicting physical properties of sand cores by simulations on digital microstructures. Int. J. Solids Struct. **188–189**, 155–168 (2020). https:// doi.org/10.1016/j.ijsolstr.2019.09.014